Yield Optimization and Time Structure of Femtosecond Laser Plasma $K\alpha$ Sources

Ch. Reich,* P. Gibbon, I. Uschmann, and E. Förster

Abteilung Röntgenoptik, Institut für Optik und Quantenelektronik, Friedrich-Schiller-Universität Jena, Max-Wien-Platz 1, D-07743 Jena, Germany

The generation of femtosecond $K\alpha$ x rays from laser-irradiated plasmas is studied with a view to optimizing photon number and pulse duration. Using analytical and numerical models of hot electron generation and subsequent transport in a range of materials, it is shown that an optimum laser intensity $I_{\mathrm{opt}} = 7 \times 10^9 Z^{4.4}$ exists for maximum $K\alpha$ yield. Furthermore, it is demonstrated that bulk targets are unsuitable for generating sub-ps x-ray pulses: instead, design criteria are proposed for achieving $K\alpha$ pulse durations ≤ 100 fs using foils of ≈ 2 μm thickness.

During the interaction of an ultra-high-intensity laser beam with a solid, a plasma is rapidly created at the surface. Collective absorption mechanisms transfer part of the laser energy into hot electrons, which are accelerated to multi-keV energies and penetrate into the "cold" solid behind the plasma, where they generate x rays via K-shell ionization and bremsstrahlung under a wide variety of experimental conditions [1,2]. These x-ray bursts offer the prospect of creating a cheap and compact source of hard x rays [3], posing a promising alternative to synchrotron radiation, e.g., in medical imaging applications [4]. At first sight, the highest intensity achievable with a given laser system should give the biggest $K\alpha$ yield, since higher laser intensities generate more hot electrons with energies above the K-shell ionization energy of the solid. However, Eder *et al.* have recently reported observing a maximum in $K\alpha$ emission when the target was placed away from the best focus [5]. Eder *et al.* qualitatively explain the existence of an optimal laser intensity with the reabsorption of produced photons inside the target: Higher laser intensities lead to electrons with higher energies and smaller cross sections, producing the $K\alpha$ photons deeper inside the target. More photons are reabsorbed on their way to the target surface, so the observed radiation drops.

In the first part of this Letter, we show that the dependence of $K\alpha$ emission on the target element is self-similar, leading to a universal value for the optimal hot electron temperature. Using this result, a simple scaling of the laser intensity giving maximum $K\alpha$ yield can be derived. These analytical predictions are then verified by numerical simulations for a wide range of laser intensities and target materials.

The unique short pulse duration of laser plasma x-ray sources opens up completely new possibilities in time-resolved measurements of ultrafast phenomena such as phase transitions, chemical reactions, and lattice dynamics [6]. Though it is clear that contemporary laser systems will *in principal* allow for x-ray experiments with femtosecond time resolution—in contrast to the ~ 2 ps achievable with state-of-the-art synchrotron-streak camera setups

[7]—it is still not known how the stopping times of the hot electrons in the solid influence the temporal development of the x-ray emission and thus the effective resolution [8]. In the second part of this Letter, we consider the temporal structure of the $K\alpha$ emission from laser plasma sources, showing that it will be difficult to generate 100 fs x-ray pulses from bulk targets. To overcome these restrictions, we propose formulas for the design of foil targets to produce high-yield hard x-ray pulses of a specific duration. Such targets have previously been considered in other contexts [9].

For the numerical modeling, a two-step approach was applied to determine the $K\alpha$ emission. First, 1D, oblique incidence particle-in-cell (PIC) simulations [10] were performed to obtain hot electron distributions $f_{\mathrm{hot}}(E)$ for density profiles appropriate to interactions where a laser prepulse or pedestal generates a small amount of preformed plasma [11]. Second, a Monte Carlo (MC) transport code [12] extended for the calculation of $K\alpha$ emission was used to compute electron trajectories in the solid. K-shell ionization cross sections from Casnati *et al.* [13] were applied together with fluorescence yields, relative line intensities, and absorption lengths for self-emitted $K\alpha$ radiation given by Zschornack [14]. Temporal information on electrons and photons was calculated taking into account the electron entry time into the solid (PIC code), the photon generation time, and the time of flight of the photon to the detector (MC code). All calculations were performed for a p-polarized, high-contrast 60 fs-Ti:Sa laser with an incidence angle of 45°, delivering a *constant energy* of 100 mJ on the target. An exponential plasma density profile with scale length $L = 0.3\lambda$, $n_e(\mathrm{max}) = 10n_c$ was used, n_c being the critical density. The $K\alpha$ radiation was "observed" normal to the target front side.

Analytically, the $K\alpha$ yield from a hot electron distribution can be expressed as an energy integral over the properties of monoenergetic electrons

$$N = \int n_{\mathrm{hot}} f_{\mathrm{hot}}(E) N_{\mathrm{gen}}(E) f_{\mathrm{em}}(E) \, dE, \qquad (1)$$

where N is the number of emitted photons, n_{hot} is the total number of hot electrons, and $f_{hot}(E)$ is their energy distribution; $N_{gen}(E)$ is the number of $K\alpha$ photons generated by an electron of incidence energy E, and $f_{em}(E)$ is the fraction of these photons that escapes from the solid—the "emission factor."

To simplify the following analysis we applied a formula slightly modified to that in Ref. [15]: $N_{gen}(E) = 4 \times 10^{-3}Z^{-1.67}E^{3/2}$, where Z is the atomic number. The numerical coefficients were found by fits to the results of MC simulations using monoenergetic electrons. (All energies are henceforth in keV.) These simulations also demonstrate that the emission factor shows a *universal behavior* with respect to the incident electron energy normalized to the K-shell ionization energy of the target: $U = E/E_k$—Fig. 1(a). At $U = 20$, the mean depth of $K\alpha$ generation in the target is comparable to the absorption length for self-emitted $K\alpha$ radiation—Fig. 1(b), so that for $U < 20$ most of the generated photons can escape from the target. For $U > 20$, the electron penetration depth and reabsorption both increase, so that f_{em} falls off rapidly as $\sim U^{-5/3}$. To facilitate the integration of Eq. (1), the emission factor was approximated by a step function:

$$f_{em} = \begin{cases} 1 & : & U \le 20, \\ 0 & : & U > 20. \end{cases} \quad (2)$$

Applying a fit of the ionization energies, we can approximate $U \approx E/0.0054Z^{2.2}$.

Analytical expressions were derived for n_{hot} and $f_{hot}(E)$ from fits to the results of PIC simulations for a range of laser intensities. We found that f_{hot} is best fitted with a one-dimensional Maxwellian energy distribution $f(E)dE = 1/\sqrt{EkT}\exp(-E/kT)\,dE$ [16]. From the PIC results we find a temperature scaling with laser intensity I as

$$kT \approx 130 \text{ keV}\sqrt{\frac{I}{10^{17}\text{ W cm}^{-2}}}, \quad (3)$$

while the number of generated electrons scales as

$$n_{hot} \approx 1.9 \times 10^{20}I^{-1/2}. \quad (4)$$

This expression takes into account the decrease of irradiated surface area $\sim I^{-1}$ with increasing laser intensity when the laser energy is kept constant. Integrating $\int n_{hot}f_{hot}(E)E\,dE$ and applying (3) for the hot electron temperature gives the total energy of the hot electrons. This product is *independent* of the laser intensity, consistent with PIC simulations which give a roughly constant (40%–60%) energy conversion into hot electrons over the range considered here.

Gathering these results together, the total $K\alpha$ yield of Eq. (1) in the interval $1 \le U \le 20$ is

$$N_{I,Z} = 3.5 \times 10^{16}\frac{Z^{2.73}}{I^{3/4}}\int_1^{20}U\exp\left(-\frac{U}{U_{kT}}\right)dU, \quad (5)$$

with the shape of the integrand being determined by the normalized electron temperature

$$U_{kT} = \frac{kT}{E_k} = 7.6 \times 10^{-5}\frac{\sqrt{I}}{Z^{2.2}}. \quad (6)$$

U_{kT} is also the electron energy at which the most $K\alpha$ photons are produced. The total $K\alpha$ yield is highest for an optimal electron temperature U_{opt}. Equation (6) therefore implies an optimal laser intensity I_{opt} for a given Z. Setting $\partial N/\partial I = 0$ gives

$$I_{opt} = 7 \times 10^9 Z^{4.4}, \quad (7)$$

which corresponds to an electron temperature $U_{opt} = 6.4$.

The scaling of I_{opt} results from the combination of two scaling laws. The reference value for $K\alpha$ production *and* reabsorption is the ionization energy of the K shell, which gives a scaling of the appropriate hot electron energy as $E \propto Z^{2.2}$. The laser intensity scales with the hot electron energy as $I \propto (kT)^2$, giving $I_{opt} \propto Z^{4.4}$. A weaker temperature scaling, e.g., $kT \propto (I\lambda^2)^{1/3}$, would lead to a correspondingly stronger scaling of I_{opt} with Z.

To check the result in (5), combined PIC-MC calculations were used to derive $K\alpha$ yields without the approximations included in the analytical model—Fig. 2(a). Photon numbers in Fig. 2(a) agree within a factor of 3 with those predicted by Eq. (5). For all elements, the $K\alpha$
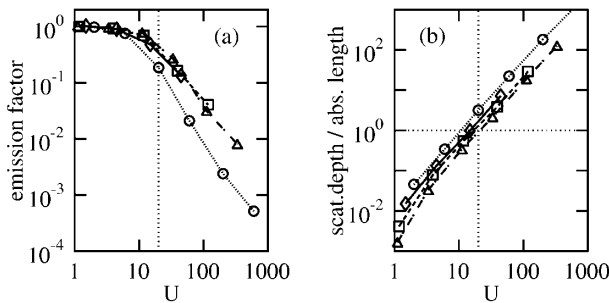

FIG. 1. (a) The emission factor f_{em} of monoenergetic electrons and (b) ratio of mean depth of $K\alpha$ generation to absorption length versus $U = E/E_k$. ○: Ti; △: Cu; □: Ag; ◇: Ta. Dotted lines: $U = 20$.
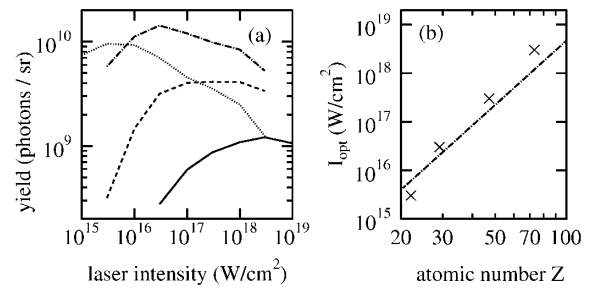

FIG. 2. (a) Simulated $K\alpha$ yields from bulk targets for a laser energy of 100 mJ: Ti (dotted line), Cu (dash-dotted line), Ag (dashed line), and Ta (solid line). (b) Dependence of the optimum laser intensity on the target material. Points are from simulations (a); the line is from the analytical model—Eq. (7).

yield shows a distinct maximum at an optimal laser intensity I_{opt}, which follows the predicted $Z^{4.4}$ dependence of Eq. (7)—Fig. 2(b). The deviations from the analytical result are due to the approximate handling of reabsorption—Eq. (2) in the model. For example, the lower simulated $K\alpha$ yield for Ti is caused by its disproportionately short absorption length, which leads to a lower optimum hot electron temperature and laser intensity. The simulated values are generally in good agreement with experimental data [17], although slightly higher. For Cu, $I_{opt} \approx 3 \times 10^{16}$ W/cm^2—a value consistent with the results reported by Eder *et al.* [5], where a peak intensity defocused to 10^{17} W/cm^2 gave a $2\times$ enhancement of $K\alpha$ yield.

Applications involving time-resolved x-ray diffractometry or spectroscopy depend critically on the *duration* of the $K\alpha$ pulse. $K\alpha$ emission starts shortly after the laser pulse hits the plasma, when the first hot electrons are generated and enter the solid. After the laser pulse has gone, it continues until the energy of the last hot electron in the solid has dropped below the K-shell ionization energy. The total duration of the x-ray emission is thus the sum of the durations of the laser pulse τ_l and of the "afterglow" emission τ_a, $\tau_x \approx \tau_l + \tau_a$. Depending on the laser intensity, a small fraction of "super-hot" electrons can produce a long-lasting $K\alpha$ afterglow with low intensity. For example, 90% of the $K\alpha$ emission from Cu, irradiated for 60 fs at $I_{opt} = 3 \times 10^{16}$ W/cm^2, occur within 400 fs, though the total emission lasts for more than 1.6 ps.

The low-intensity emission from the "tail" will have a negligible influence on observations. Thus, we define the time of the first 90% of emission (instead of its shorter FWHM) as the temporal figure of merit of the $K\alpha$ pulses, this being the time scale which can be resolved in experimental applications. With increasing laser intensity, the $K\alpha$ pulse duration increases because the higher electron temperature implies longer afterglow emission—Fig. 3. Inspection of Figs. 3 and 2(a) shows that, except for the lightest elements, it will be very difficult to generate efficient 100 fs $K\alpha$ pulses from bulk targets suitable for ultrafast diagnostic applications.

Afterglow emission can be restricted by using *foil* targets, which are quickly traversed by super-hot electrons, limiting the time they can produce x rays [18]. To calculate the foil thickness and laser intensity needed we look for the electron energy E_{max} which gives maximum $K\alpha$ emission for a given τ_a and subsequently assume that, as in the bulk case, the *optimal* laser intensity generates a hot electron temperature equal to E_{max}. The number of photons which an electron can produce depends on the time it spends inside the target. With increasing incidence energy, this excursion time initially increases, since faster electrons need more scattering events to lose their energy. When the electrons are energetic enough to traverse the foil, the *mean* time spent inside the target decreases again with increasing energy. Thus, there is an optimal electron
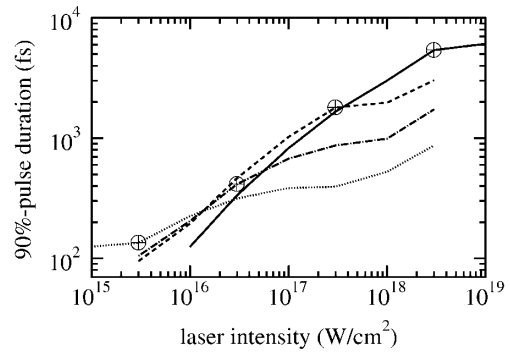

FIG. 3. Simulated 90% $K\alpha$ pulse durations from bulk targets: Ti (dotted line), Cu (dash-dotted line), Ag (dashed line), and Ta (solid line). The crosses mark the optimal laser intensities for each element.

energy E_{max} which gives maximum mean excursion time inside the target τ_{max}, and therefore a maximum number of $K\alpha$ photons per incidence electron energy. To determine how E_{max} and τ_{max} depend on target material and target thickness l, numerical simulations using monoenergetic electrons were again applied, giving

$$E_{max} \approx 1.1 Z^{0.95} l^{0.5}, \qquad (8)$$

$$\tau_{max} \approx 100 Z^{-0.4} l^{0.8}, \qquad (9)$$

where the units are fs, μm, and keV. The electrons with $E = E_{max}$ give an afterglow emission with duration $\tau_a \sim \tau_{max}$. Then the foil thickness [Eq. (9)] and the laser intensity [Eqs. (3), (8), and (10)] must be chosen as

$$l = 0.0032 Z^{0.5} (\tau_x - \tau_l)^{1.25}, \qquad (10)$$

$$I_{opt} = 2.3 \times 10^{10} Z^{2.4} (\tau_x - \tau_l)^{1.25}. \qquad (11)$$

Table I gives an overview of the parameters predicted by (10) and (11) for a desired x-ray pulse duration of 100 fs, taking into account the 60-fs-laser pulse.

Simulations using realistic hot electron distributions from the PIC code together with parameters calculated from Eqs. (10) and (11) yield 90%-pulse durations a little lower than 100 fs (Table I). With increasing foil thickness, both the $K\alpha$ yield and the pulse duration increase, though the duration does not depend critically on the thickness—Fig. 4(a). For the foil thickness giving just a pulse duration of 100 fs, the $K\alpha$ yield does in fact show a

TABLE I. Calculated parameters of foil targets for the generation of 100 fs $K\alpha$ pulses; simulated $K\alpha$ pulse duration τ_x (first 90% of emission) and $K\alpha$ yield for calculated l and I_{opt}.

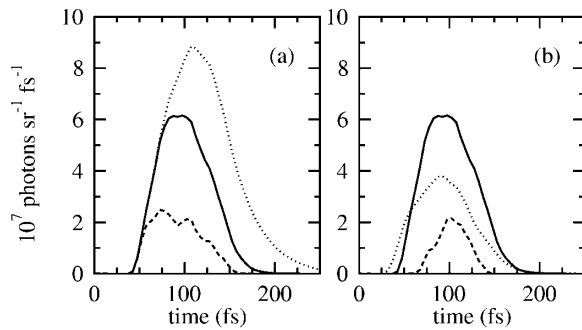| Element	Z	l (μm)	I_{opt} (W/cm^2)	τ_x (fs)	Yield (photons/sr)
Ti	22	1.5	4×10^{15}	90	5×10^9
Cu	29	1.7	7×10^{15}	90	5×10^9
Ag	47	2.2	3×10^{16}	95	6×10^8
Ta	73	2.8	7×10^{16}	95	7×10^7

FIG. 4. $K\alpha$ emission from Cu foils: (a) Irradiated at $I = 7 \times 10^{15}$ W/cm^2, for thicknesses: 0.5 μm (dashed line), 1.7 μm (solid line), and 5 μm (dotted line). (b) For constant thickness: 1.7 μm, irradiated 10^{15} W/cm^2 (dashed line), 7×10^{15} W/cm^2 (solid line), and 3×10^{16} W/cm^2 (dotted line).

distinct maximum at the calculated laser intensity. Again the pulse duration increases only slowly with increasing laser intensity—Fig. 4(b). The combination of fewer scattering events in foil targets and reduced optimal laser intensity, producing fewer electrons with $U > 1$, implies a loss in $K\alpha$ yield compared to bulk targets of a factor of $\sim$2 for Ti and up to $\sim$15 for Ta.

The MC simulations show that under these conditions more than 30% of the hot electrons pass through the target, implying the creation of a space charge—Eq. (4), which would cause a considerable number of electrons to return into the target and produce radiation again. This effect can be mitigated by a second massive layer of conducting material behind the $K\alpha$ producing foil to supply a return current, compensating the current of the impinging hot electrons and thus keeping the foil electrically neutral [18]. Simulations using carbon as the "neutralizing material" show that this target design stretches the 90%-pulse duration to 95 fs for Ti and 140 fs for Ta due to electrons backscattered from the carbon layer.

In summary, we have presented a systematic study of femtosecond $K\alpha$ sources, giving formulas for the optimal photon yield and pulse duration which agree well with the results of PIC-MC simulations. In biomedical imaging applications [4], the maximum achievable magnification will be limited by source broadening—whether caused by lateral transport, in both plasma and solid [5,19], or by deliberate laser defocusing. In practice, therefore, a compromise must be found between small source size and optimum photon yield, an issue for future study.

*Email address: reich@roentgen.physik.uni-jena.de

[1] See, for example, P. Gibbon and E. Förster, Plasma Phys. Controlled Fusion **38**, 769 (1996), and references therein.

[2] H. Chen *et al.,* Phys. Rev. Lett. **70**, 3431 (1993); M. Schnürer *et al.,* J. Appl. Phys. **80**, 5604 (1996); T. Feurer *et al.,* Phys. Rev. E **56**, 4608 (1997).

[3] J. C. Kieffer *et al.,* Phys. Fluids B **5**, 2676 (1993); A. Rousse *et al.,* Phys. Rev. E **50**, 2200 (1994).

[4] S. Svanberg, J. Larsson, A. Persson, and C.-G. Wahlström, Phys. Scr. **49**, 187 (1994).

[5] D. C. Eder *et al.,* Appl. Phys. B **69**, published online: http://dx.doi.org/10.1007/s003409900098 (1999).

[6] C. Rischel *et al.,* Nature (London) **390**, 490 (1997); C. W. Siders *et al.,* Science **286**, 1340 (1999); F. Raksi *et al.,* J. Chem. Phys. **104**, 6066 (1996); C. Rose-Petruck *et al.,* Nature (London) **398**, 310 (1999).

[7] J. Larsson *et al.,* Opt. Lett. **22**, 1012 (1997).

[8] J. Kieffer *et al.,* J. Opt. Soc. Am B **13**, 132 (1996); B. Soom, H. Chen, Y. Fisher, and D. D. Meyerhofer, J. Appl. Phys. **74**, 5372 (1993).

[9] L. Gizzi *et al.,* Phys. Rev. Lett. **76**, 2278 (1996); A. Andreev *et al.,* Appl. Phys. B **69**, published online: http://dx.doi.org/10.1007/s003409900154 (1999).

[10] P. Gibbon *et al.,* Phys. Plasmas **6**, 947 (1999).

[11] S. Bastiani *et al.,* Phys. Rev. E **56**, 7179 (1997).

[12] D. C. Joy, *Monte Carlo Modeling for Electron Microscopy and Microanalysis* (Oxford University Press, Oxford, 1995).

[13] E. Casnati, A. Tartari, and C. Baraldi, J. Phys. B **15**, 155 (1982).

[14] G. Zschornack, *Atomdaten für die Röntgenspektralanalyse* (Deutscher Verlag für Grundstoffindustrie, Leipzig, 1989).

[15] M. Green and V. Cosslett, J. Phys. D **1**, 425 (1968).

[16] C. Kittel, *Elementary Statistical Physics* (Wiley, New York, 1961).

[17] T. Schlegel *et al.,* Phys. Rev. E **60**, 2209 (1999); J. Yu, Z. Jiang, and C. Kieffer, Phys. Plasmas **6**, 1318 (1999).

[18] D. von der Linde (private communication).

[19] T. Feurer *et al.,* in *Applications of High Field and Short Wavelength Sources VIII* (OSA, Washington, DC, 1999), pp. 108–110.